

# Are arrhythmic hearts more complex ? Using skewness and the first-digit phenomenon to identify dynamical transitions in cardiac models

Pavithraa Seenivasan<sup>1</sup>, Soumya Easwaran<sup>1</sup>, S. Sridhar<sup>1,2</sup> and Sitabhra Sinha<sup>1</sup>

<sup>1</sup>*The Institute of Mathematical Sciences, CIT Campus, Taramani, Chennai 600113, India.*

<sup>2</sup>*Scimergent Analytics and Education Pvt Ltd, Adyar, Chennai, India.*

(Dated: December 7, 2024)

Disruptions in the normal rhythmic functioning of the heart, termed as arrhythmia, often result from qualitative changes in the excitation dynamics of the organ. The transitions between different types of arrhythmia are accompanied by alterations in the spatiotemporal pattern of electrical activity that can be measured by observing the time-intervals between successive excitations of different regions of the cardiac tissue. In this paper we show that the distribution of these time-intervals exhibit a systematic change in their skewness during such dynamical transitions. Further, the leading digits of the normalized intervals appear to fit Benford's law better at these transition points. This raises the possibility of using these observations to design a clinical indicator for identifying changes in the nature of arrhythmia. More importantly, our results reveal an intriguing relation between the changing skewness of a distribution and its agreement with Benford's law, both of which have been independently proposed earlier as indicators of regime shift in dynamical systems. Our results also indicate that transitions to more irregular behavior of cardiac activity is accompanied by increasing dynamical complexity as measured by multifractal analysis. As our simulation study does not involve any autonomic modulation of cardiac activity, it suggests a possibly critical role played by the nervous system in making the dynamics of the healthy heart appear more complex than diseased ones as reported by ECG studies of heart rate dynamics.

PACS numbers: 87.19.Hh,05.45.-a

## I. INTRODUCTION

Many vital physiological processes are characterized by rhythmic activity, ranging from the circadian clock regulating the daily sleep-wake cycle to temporal patterns of respiration that occur over a scale of seconds [1]. The periodic beating of the heart, that results in constant circulation of oxygenated blood throughout the body, is one of the most important of such naturally occurring oscillatory phenomena in the body [2]. Certain types of disturbances in the cardiac rhythmicity, referred to as arrhythmia, can severely impair the normal functioning of the heart and in the most critical instances, can result in sudden cardiac death [3]. Such "dynamical diseases" [4], i.e., diseases resulting from abnormal activity in an otherwise intact physiological system, are a significant public health burden in developed countries. For example, in the United States, diseases of the heart constitute the leading cause of death (responsible for about 25% of all deaths), of which more than half can be classified as sudden cardiac deaths [5–7]. Even in developing countries, in recent times heart disease has overtaken other causes of death, e.g., sudden cardiac deaths contributed to about 10% of overall mortality in certain regions in India, accounting for upto half of all cardiovascular-related deaths [8, 9].

Several studies have shown that early detection of onset of arrhythmia resulting in prompt therapeutic intervention significantly improves the chances of surviving such episodes [10, 11]. Thus, developing methods for identifying signs of impending arrhythmic events with

potentially serious consequences can significantly contribute towards reducing the mortality rate due to sudden cardiac death. With this aim in view there have been a number of attempts at applying time-series analysis methods on cardiac activity data in order to extract robust indicators of imminent instances of temporal irregularities in the heart. However, the complexity of heart rate dynamics makes it difficult to characterize and distinguish the temporal signatures of a healthy heart from a diseased one [12–15].

Most studies of cardiac time-series have focused on heart rate variability as measured by temporal changes in the *R-R interval*, the duration between successive episodes of ventricular depolarization which triggers contraction of the lower chambers of the heart. Following the pioneering observations connecting decreased variance in R-R intervals with higher mortality risk in patients suffering myocardial infarction [16, 17], it is now generally accepted that healthy individuals have higher heart-rate variability compared to those with diseased hearts [18]. However, certain pathological conditions including cardiac arrhythmia are seen to be extremely irregular [19]. In fact, it has been observed that a transition from tachycardia, i.e., abnormally rapid heart-rate, to fibrillation, characterized by erratic muscle activity that prevents the heart from pumping blood, is marked by a switch from relatively more periodic activity to a highly irregular dynamical state [20]. While the R-R intervals in normal sinus rhythm appear to have almost as unpredictable a nature as that seen during fibrillation [21], it has been suggested that the "chaoticity" during normal cardiac activity arises through interaction of the heart with the ner-

nous system [22]. In contrast, the spatiotemporal chaos associated with fibrillation arise from intrinsic instabilities in cardiac excitation dynamics [23].

One possible route from tachycardia to fibrillation that has been established through extensive simulation studies of models of cardiac electrical activity is the degeneration of reentrant spiral wave (corresponding to tachycardia) to disordered, turbulent activity (characterizing fibrillation) through spiral breakup [24, 25]. This dynamical transition has been reproduced in a wide range of systems, from simple, excitable media to biologically detailed models, underlining the robustness of the scenario [26]. Thus, the study of spatiotemporal dynamics in models of electrical activity in cardiac tissue provides another perspective to identify indicators for an impending onset of possibly life-threatening arrhythmia.

In this paper, we focus on analyzing time-series data obtained from spatially extended models of cardiac ventricular activity in which, by tuning specific physiological parameters, one can observe transitions to different dynamical regimes representing various classes of arrhythmia. This allows us to look for statistical signatures that can help in early detection of arrhythmic episodes, where the observed patterns are exclusively due to abnormal excitation activity that characterizes such arrhythmia and unrelated to heart rate variability that arises from the influence of the nervous system on the sinus node, the natural pacemaker of the heart [27]. This study, therefore, provides a benchmark against which analysis of ECG data obtained from clinical studies can be compared, enabling distinction of statistical features of arrhythmic time-series that are intrinsic to the dynamics of heart muscle from those that are a result of changes in the autonomic modulation of cardiovascular function (achieved through dynamical balance between sympathetic and parasympathetic effects [28]). As signature patterns (if they exist) that indicate transitions from one dynamical regime of cardiac activity to another may be masked by other effects in reality, establishing them through analysis of the model output will allow us to look for them in data obtained from experimental or clinical studies.

Here, for our statistical analysis, we have focused on the sequence of time-intervals  $T$  between successive excitations of ventricular muscle cells (analogous to the R-R interval for ECGs) as a representative feature of heart rate dynamics (Fig. 1). An important result of our study is that the distribution of these intervals exhibit clearly observable changes in their moments - in particular, the skewness - around the onset of qualitatively distinct dynamical behavior characterizing various arrhythmic episodes (represented by the different panels in Fig. 1). Intriguingly, we also observe that at these transitions, the distribution of the time-intervals appears to agree better with Benford's law (BL), an empirically established feature of the frequency distribution of leading digits of numbers occurring in many phenomena in various physical, biological and social contexts [29–32].

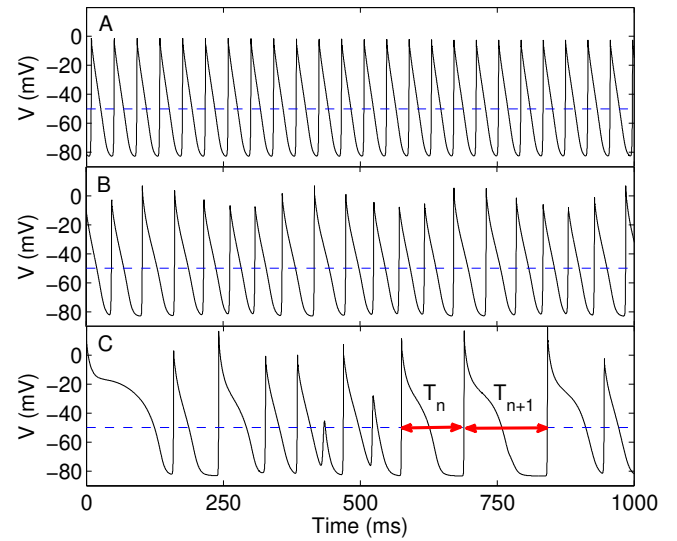


FIG. 1: Time-series of the transmembrane potential  $V$  representing local excitation activity in a two-dimensional LR1 model ( $L = 400$ ) for different values of the maximum  $\text{Ca}^{2+}$  channel conductance  $G_{si}$ , viz., (A) 0.005, (B) 0.04 and (C)  $0.065 \text{ mS cm}^{-2}$ . The distinct nature of the corresponding spatiotemporal dynamics, viz., rigid rotation of a spiral similar to monomorphic tachycardia (A), chaotic meandering of spiral core representing polymorphic tachycardia (B), and spatiotemporal chaos indicating fibrillation (C), is visually apparent in the varying pattern of intervals between successive excitations. It is quantified in terms of the sequence of time-intervals  $\{T_n\}$  ( $n = 1, 2, \dots$ ) between each pair of consecutive local supra-threshold depolarizations (two such intervals are shown in panel C using double-headed arrows). We consider a local supra-threshold excitation event to have occurred when  $V$  exceeds  $-50 \text{ mV}$  (broken line).

Both variation in skewness [33, 34] and closer agreement with BL [35] have independently been suggested as indicators of regime shifts or phase transitions in different systems. Our work not only finds both of these signatures to be indicative of the onset of arrhythmic behavior, but additionally suggests that these two phenomena (viz., increasing skewness and agreement with BL) may be related.

## II. MATERIALS AND METHODS

**Model.** To simulate spatiotemporal excitation activity in cardiac muscle under different physiological conditions, we have used a two-dimensional model of ventricular tissue having the generic form

$$\frac{\partial V}{\partial t} = \frac{-I_{ion}(V, g_i)}{C_m} + D \nabla^2 V, \quad (1)$$

where  $V$  (mV) is the potential difference across a cellular membrane,  $C_m$  ( $= 1 \mu\text{F cm}^{-2}$ ) is the transmembrane

capacitance,  $D$  is the diffusion constant ( $= 0.001 \text{ cm}^2 \text{ s}^{-1}$  for the results reported in the paper),  $I_{ion}(\mu \text{A cm}^{-2})$  is the total current density through ion channels on the cellular membrane, and  $g_i$  describes the dynamics of gating variables of different ion channels. The specific functional form for  $I_{ion}$  used here is that of the Luo-Rudy I (LR1) model that describes the ionic currents in a guinea pig ventricular cell [36]:

$$I_{ion} = I_{Na} + I_K + I_{K1} + I_{Kp} + I_{si} + I_b,$$

where  $I_{Na} = G_{Na}m^3hj(V - 54.4)$  is the fast inward  $\text{Na}^+$  current,  $I_{si} = G_{si}df(V - E_{si})$  is the slow inward  $\text{Ca}^{2+}$  current where  $E_{si} = 7.7 - 13.0287 \ln([{\text{Ca}^{2+}}]_i)$  is the reversal potential, dependent on the intracellular ion concentration  $[\text{Ca}^{2+}]$ ,  $I_K = G_Kxx_1(V + 77.62)$ ,  $I_{K1} = G_{K1}K_{1\infty}(V + 87.95)$  and  $I_{Kp} = 0.0183Kp(V + 87.95)$  are three different types of  $\text{K}^+$  current, and  $I_b = 0.03921(V + 59.87)$  is a background current. The currents are determined by ion channel gating variables  $m$ ,  $h$ ,  $d$ ,  $f$  and  $x$ , whose time evolution is described by ordinary differential equations of the form,  $d\epsilon/dt = (\epsilon_\infty - \epsilon)/\tau_\epsilon$ , where  $\epsilon_\infty$  is the steady state value of  $\epsilon$  ( $= m$ ,  $h$ ,  $d$ ,  $f$  and  $x$ ) and  $\tau_\epsilon$  is the corresponding time constant obtained by fitting experimental data. Parameter values used are as in Ref. [36], except for  $G_K$  which is set to  $0.705 \text{ mS}/\mu\text{F}$  and  $G_{si}$  that is varied to alter the stability of spiral wave dynamics [37].

For numerical simulations, the two-dimensional spatially extended system is discretized on a grid of size  $L \times L$  ( $L = 400$ ) with a space step of  $\delta x = 0.0225 \text{ cm}$ . The equations are solved using a forward Euler method with time step  $\delta t = 0.05 \text{ ms}$  and a standard 5-point stencil for the Laplacian describing the spatial coupling between the lattice elements. No-flux boundary conditions are implemented at the edges. The initial spiral wave state is obtained by generating a broken wave front which then dynamically evolves into a curved rotating wave. The movement of the spiral wave core is obtained by tracing the trajectory of intersection points of iso-contour lines for a pair of dynamical variables of the model, viz.,  $V$  and  $h$  [38].

**Multifractality.** We have characterized the dynamical complexity of spatiotemporal activity in different parameter regimes by analyzing the multifractal character of the corresponding fluctuation behavior in the membrane potential ( $V$ ) at local regions. We use the multifractal detrended fluctuation analysis (MFDFA) technique for this purpose, with the fluctuations in short segments of length  $t$  of the time-series for  $V$  being obtained after eliminating the average trend over the segments [39]. The  $q$ -th order Hurst exponent  $h(q)$  is determined as a power-law exponent of the  $q$ -th order fluctuation function  $F_q(t)$  expressed as a function of the scale  $t$ , viz.,  $F_q(t) \sim t^{h(q)}$ . We next obtain the scaling exponent function  $\tau(q)$  which is related to the  $q$ -th order Hurst exponent as  $\tau(q) = qh(q) - 1$  [39]. The local singularity exponent  $\alpha$  and its spectrum  $f(\alpha)$  is calculated by a Legendre transform as  $\alpha = \frac{d\tau(q)}{dq}$  and  $f(\alpha) = q\alpha - \tau(q)$  [39].

**Inter-spike interval time-series.** We analyze the statistical properties of the time-intervals between successive excitations (i.e., depolarization) of a local region. For this purpose, each point in the simulation domain is considered to be excited if the corresponding transmembrane potential  $V$  crosses a threshold value (set equal to  $-50 \text{ mV}$  here, although our results are robust with respect to the choice of threshold) from below, i.e., from a hyperpolarized state. The time-interval  $T$  between two such successive crossings of the threshold is recorded for constructing the data-set, values being sampled from a large number of regularly spaced points on the simulation domain. We have avoided using data from points in the vicinity of the vortex as, close to the phase singularity at the spiral core, artifacts enter the calculation of the time-interval. From the data-sets obtained at different values of  $G_{si}$ , the corresponding distributions for  $T$  are obtained and the moments calculated, including mean  $\mu$ , standard deviation  $\sigma$ , and skewness, the latter being measured by the Pearson's moment coefficient of skewness defined as  $\gamma = E[(X - \mu)/\sigma]^3$ . Using other measures for the skewness did not qualitatively alter our results. The time-interval distributions obtained for different parameters are also tested for the degree of agreement with Benford's Law.

**BL and Benford distribution.** Named after the American physicist F. Benford who made the first-digit phenomenon widely known, BL had been noticed in numbers associated with a variety of natural (as well as social) phenomena as far back as in 1881 by the astronomer S. Newcomb. According to this empirical law, numbers beginning with 1 or 2 occur more often than those beginning with 8 or 9 [40]. Specifically, the probability of the first or leading digit of such numbers being  $i$  ( $i = 1, 2, \dots, 9$ ) is given by the *Benford distribution*:

$$P(i) = \log_{10} \left( 1 + \frac{1}{i} \right).$$

The reason for the ubiquity of this distribution has been connected to its scale-invariance and base-invariance [41]. Thus, if indeed there is a universal principle underlying the distribution of the leading digits of numbers which is independent of the units in which the numbers are measured or the number base used, then the BL follows. Simple mathematical arguments have been used to show that any distribution of numbers arising from natural processes that spans several orders of magnitude and is reasonably smooth will obey BL [40]. The Benford distribution, as mentioned earlier, is seen in many empirical data-sets, including those arising in a biological context, such as, the distribution of open reading frames in prokaryotic and eukaryotic genomes [31]. Dynamical systems, such as those describing the molecular dynamics of fluids or certain chaotic systems, also exhibit BL in the numbers expressing coordinates of the generated trajectories [42, 43]. More recently, BL has been used as a signature for detecting phase transitions in a quantum system [35].

In order to compare the distribution of the intervals  $T$  between successive excitations with that expected from BL, we first obtain a set of normalized time-intervals  $t$  by subtracting the minimum value of the series from all intervals  $T$  and dividing by the range, i.e.,  $t = [T - \min(T)]/[\max(T) - \min(T)]$ . The leading digits  $i$  of the normalized intervals  $t$  are then extracted as  $i = \lfloor |t|/10^{\lfloor \log_{10}(|t|) \rfloor} \rfloor$ , where  $|z|$  and  $\lfloor z \rfloor$  indicate the absolute value of  $z$  and the largest integer not greater than  $z$  respectively. The distribution of  $i$  is then tested for agreement with BL using statistical tests for goodness of fit.

**Statistical tests for goodness of fit with BL.** The goodness of fit between the two distributions (the empirical and that predicted by BL) is measured by a two-sample Kolmogorov-Smirnov test. We have used the function *kstest2* implemented in *MATLAB* which returns a test decision for the null hypothesis that both the sets are from the same distribution, along with a  $p$ -value and the KS test statistic  $k$  describing the degree of deviation from BL. In our study the test statistic is the comparison parameter

$$k = \max_i (F_c(i) - B_c(i)),$$

which measures the maximum distance between the two cumulative distributions,  $F_c(i)$  and  $B_c(i)$ , of the leading digits  $i$  of normalized time intervals and that expected from BL, respectively. A lower value of  $k$  implies closer agreement with the Benford distribution.

Apart from the KS test, we have also used the Pearson's chi-squared test to confirm the compliance of the empirical distributions with BL. The test statistic

$$\chi^2 = \sum_{j=1}^n \frac{(F_j - B_j)^2}{B_j},$$

quantifies the total magnitude (over all  $n$  entries of the empirical time-series) of the difference between the two probability distributions,  $F$  and  $B$ , for the leading digits of the normalized time intervals and that expected from BL, respectively. As for the KS test, a lower value of  $\chi^2$  implies closer agreement with the Benford distribution.

### III. RESULTS

To identify the statistical signatures characterizing dynamical transitions to different types of arrhythmia, we systematically explore the spatiotemporal dynamics of the model system in different parameter regimes. The nature of the excitation activity is varied in a controlled manner by changing the kinetic properties of an ion channel, viz., increasing the maximum  $\text{Ca}^{2+}$  channel conductance  $G_{si}$  (keeping all other model parameters unchanged) which is known to result in a succession of dynamical transitions [44] as seen in Fig. 1. The increasing

complexity of the time-series accompanying these transitions can be quantified by multifractal analysis. As expected for time-series obtained from a stationary process, Fig. 2 (A) shows that the  $q$ -th order Hurst exponent  $h(q)$  monotonically decreases with the moment order  $q$ . The difference between the maximum and the minimum values of  $h(q)$  is considered to be a measure of the degree of multifractality. As we note from Fig. 2 (A), the difference is largest for the situation corresponding to spatiotemporal chaos and lowest for the case of a rigidly rotating spiral. The deviation from linearity of the scaling exponent function  $\tau(q)$  [Fig. 2 (B)] is widely used to indicate the degree of multifractality, with monofractal series having long-range correlations characterized by a linear dependence of  $\tau(q)$  on  $q$  [45]. The difference between the minimum and maximum of the local singularity exponent  $\alpha$ ,  $\Delta = \alpha_{\max} - \alpha_{\min}$ , quantifies the width of the multifractal spectrum, i.e., the  $f(\alpha)$  curve [Fig. 2 (C)]. The larger the  $\Delta$ , the stronger the multifractality and thus, the degree of nonlinearity of the underlying process generating the data [45]. As can be seen from Fig. 2 (C), width of the multifractality spectrum increases with irregularity of the dynamical behavior as a rigidly rotating spiral goes through increasing degree of meandering to eventually break up into a spatiotemporally chaotic state.

Representative images of the spatiotemporal dynamics in the different regimes are shown in the top row of Fig. 3, with the trajectory of the spiral core (traced in the first three panels using a light color) exhibiting characteristic changes in its qualitative nature. Starting from an initial state characterized by a rotating spiral wave, for small values of the conductance (e.g.  $G_{si} = 0.005$ ) we observe rigid rotation with the core moving around an approximately circular trajectory (Fig. 3 A), which corresponds to the clinical phenomenon of monomorphic tachycardia. This gives way to meandering at higher values of  $G_{si}$  ( $\simeq 0.025$ , see Fig. 3 B), followed by the appearance of chaotic meandering around  $G_{si} = 0.04$  (Fig. 3 C) and finally the breakup of spiral waves leading to spatiotemporal chaos, representative of fibrillation, for values of  $G_{si} > 0.055$  (Fig. 3 D).

The panels in the middle row of Fig. 3 show the probability distribution of time intervals between successive excitations,  $T$ , for the  $G_{si}$  values corresponding to the panels in the top row. We observe that the range of these intervals become broader at larger  $G_{si}$  values as the dynamics of the spiral wave becomes more complex. A very narrow range of intervals is dominant at low  $G_{si}$ , as expected for a rigidly rotating spiral wave having a characteristic period of rotation (Fig. 3 E). With increased meandering of the core, however, the time interval between successive excitations of a local region becomes more irregular, which is manifested as a broader distribution of  $T$  (Fig. 3 F). As the spiral core trajectory becomes even more complex, covering a larger portion of the simulation domain, we see that the distribution not only widens further but also develops multiple peaks at the extremities (Fig. 3 G). Finally, following breakup and spatiotempo-

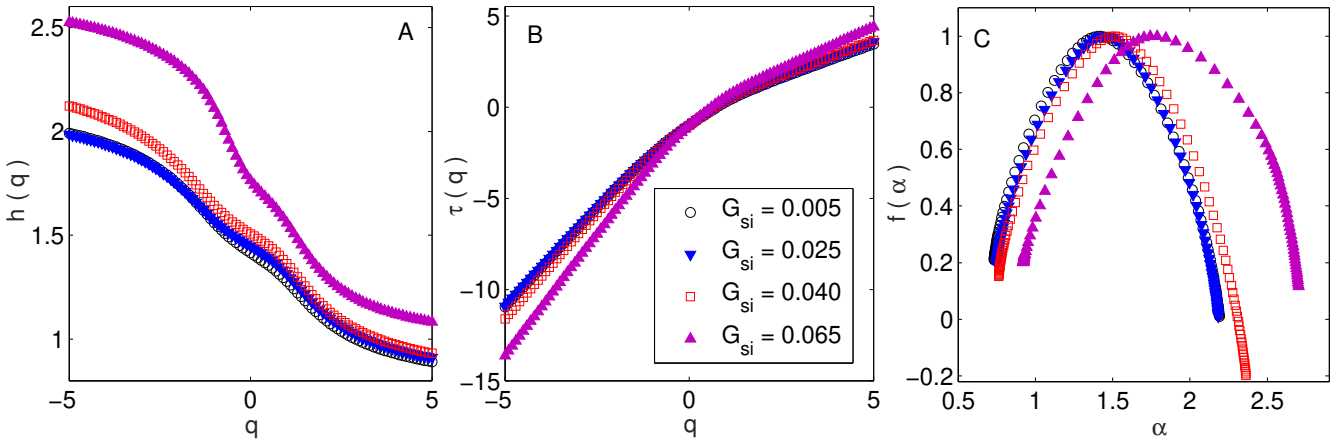


FIG. 2: Multifractal analysis using the MF-DFA (Multifractal detrended fluctuation analysis) method of the time-series for membrane potential  $V$  at a local region in simulated cardiac tissue for different dynamical regimes obtained by increasing the maximum  $\text{Ca}^{2+}$  channel conductance  $G_{si}$ . The curves obtained for the different  $G_{si}$  values are represented by symbols indicated by the key provided in panel (B). (A) The  $q$ -th order Hurst exponent  $h(q)$  decreases monotonically with the moment order  $q$ , the difference between minimum and maximum values rising with increasing disorder in the spatiotemporal activity as  $G_{si}$  is increased. This indicates that the multifractal character of the dynamics is becoming stronger as the spiral transits from rigid rotation, through quasiperiodic and chaotic meandering, to breakup. This is corroborated by the nonlinear character of the dependence of scaling exponent function,  $\tau(q)$  on  $q$ , shown in panel (B). (C) The width of the multifractal spectrum  $f(\alpha)$  of the singularity exponent  $\alpha$ , another indicator of the degree of multifractality, is also seen to increase with dynamical disorder. All data points shown are averaged over  $> 2 \times 10^3$  values.

ral chaos, the time between successive excitations become essentially random in character with a distribution that spans a relatively large range of  $T$  (Fig. 3 H).

To see how closely the dynamical process follows the Benford distribution in the different regimes, in the bottom row of Fig. 3 we show the probability distributions of the leading digits  $i$  of the normalized intervals  $t$ . It is evident that the distribution of  $i$  moves closer to the form expected for the Benford distribution (indicated by a broken curve) at larger values of  $G_{si}$ . In fact, the empirical distribution shows the best agreement with BL in the spatiotemporally chaotic state corresponding to  $G_{si} = 0.065$  (Fig. 3 L), which is consistent with the corresponding time interval distribution being exponential in nature - as it is known that values distributed exponentially follow BL. We see that that this distribution of leading digits  $i$  is closest to BL at the transition points corresponding to chaotic meandering ( $G_{si} = 0.040$ ) and spiral breakup ( $G_{si} = 0.065$ ).

To understand the nature of the distributions in the different dynamical regimes better, we show how the moments of the distribution for the time intervals  $T$  and that for the corresponding leading digits  $i$  of the normalized intervals vary with increasing  $G_{si}$  (Fig. 4). We observe that the mean value of the interval between successive excitations steadily rises with  $G_{si}$  as the complexity of the spiral core trajectory increases excepting for a small dip around  $G_{si} = 0.055$  which is the point of transition to spiral breakup (Fig. 4 A). The dispersion of the  $T$  distribution, measured by its standard deviation  $\sigma_T$

(Fig. 4 B) shows a similar increasing nature with  $G_{si}$  although, around  $G_{si} = 0.04$ , where a transition occurs from quasiperiodic to chaotic meandering of the spiral core, there is a small decrease. The skewness  $\gamma$  of the distribution is the most informative of all the moments considered here, as it shows large deviations from zero only around critical values of  $G_{si}$  associated with transitions between different dynamical regimes. In particular, we notice peaks in the skewness at  $G_{si} = 0.025, 0.04$  and  $0.055$  which correspond to transition to quasiperiodic meandering, chaotic meandering and spiral breakup, respectively (Fig. 4 C). In order to make the relation between the different moments and the dynamical transitions even more clear, we have also shown the nature of variation of a derived quantity,  $\exp(\gamma_T)/\sigma_T$ , as a function of  $G_{si}$ . It can potentially be used as a statistical indicator for the onset of certain types of arrhythmia that may be hard to detect by observing the skewness alone. We see from Fig. 4 (D) that the measure amplifies the signal indicating a transition close to  $G_{si} = 0.025$  where the spiral begins to noticeably meander.

When we observe the corresponding moments for the distribution of leading digits  $i$  as a function of  $G_{si}$ , we note that both the moments  $\mu_i$  and  $\sigma_i$  (Fig. 4 E-F) have very similar nature of variation, viz., both exhibit dips around the values of  $G_{si}$  at which the different dynamical transitions occur. In contrast, the skewness exhibits an almost opposite nature, with peaks occurring at the transition points (consistent with increasing skewness of the  $T$  distribution at these values). This indicates that at

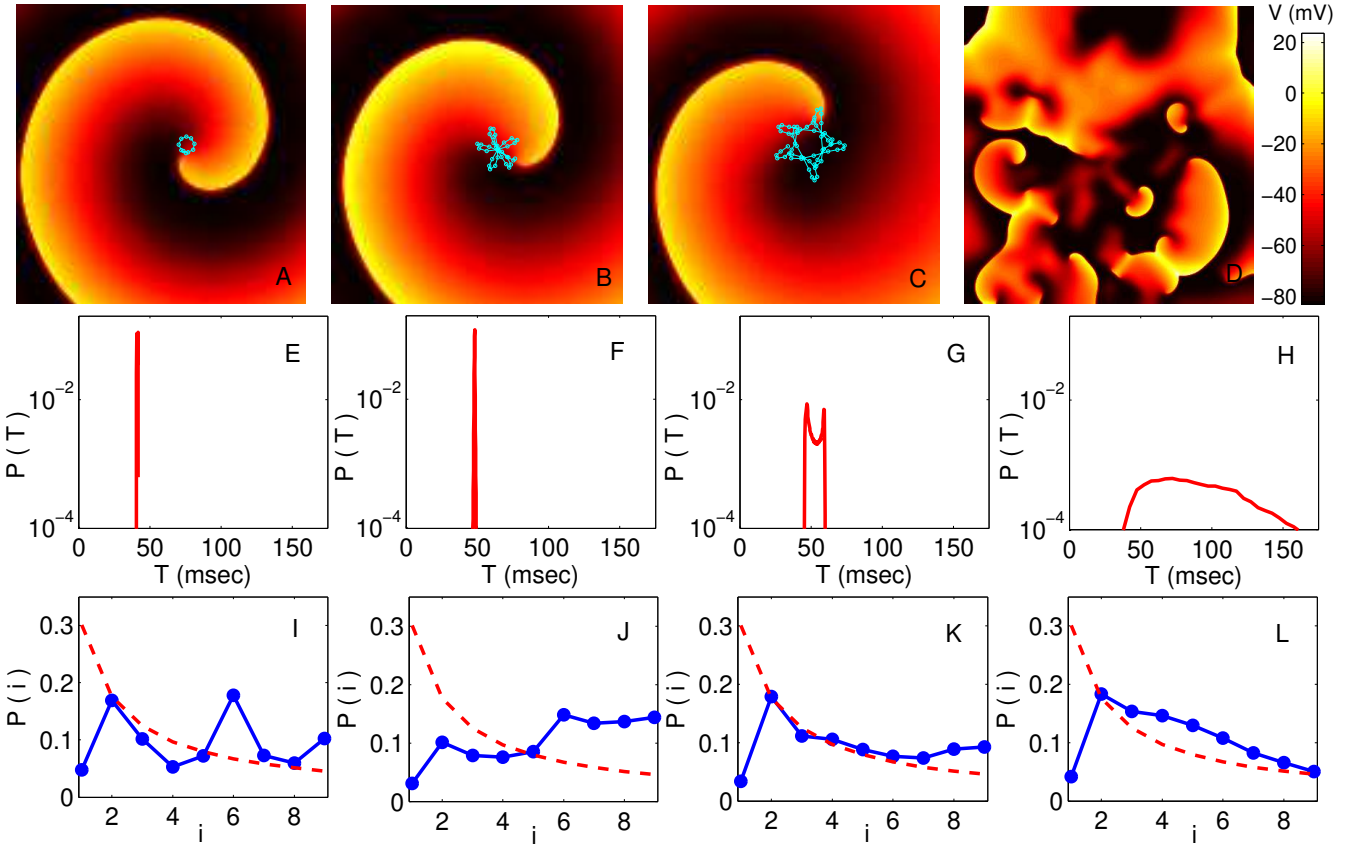


FIG. 3: (A-D) Pseudocolor images of spatiotemporal activity (measured in terms of transmembrane potential  $V$ ) for the two-dimensional LR1 model ( $L = 400$ ) showing the different dynamical regimes obtained by increasing the maximum  $\text{Ca}^{2+}$  channel conductance  $G_{si}$  (expressed in units of  $\text{mS cm}^{-2}$ ). The successive panels represent a spiral wave undergoing (A) stable rotation ( $G_{si} = 0.005$ ), (B) quasiperiodic meandering ( $G_{si} = 0.025$ ) and (C) chaotic meandering ( $G_{si} = 0.04$ ). Further increase of  $G_{si}$  results in breakup of the spiral wave resulting in (D) spatiotemporal chaos ( $G_{si} = 0.065$ ). The trajectory of the spiral core (the tip of the spiral wave, defined to be a phase singularity) for 500 ms is indicated in all panels except for the one corresponding to chaotic activity where there is a large multiplicity of singularities. (E-H) The probability distribution of time intervals  $T$  between successive supra-threshold activations of a local region corresponding to the dynamical regimes indicated in panels (A-D) respectively. Each distribution is obtained by averaging over many regions across the simulation domain and also over several realizations. (I-L) Probability distribution of the leading digits  $i$  of the normalized time intervals between successive supra-threshold activations of a local region corresponding to the dynamical regimes indicated in panel (A-D) respectively. Each distribution is obtained by averaging over many regions across the simulation domain and also over several realizations. The broken curve indicates the distribution predicted by Benford's law.

these points the distribution comes close to the form expected from BL, as the latter is associated with positively skewed distributions. The derived quantity  $\exp(\gamma_i)/\sigma_i$  conserves this pattern, showing increased values at these points. We find that the skewness of  $T$  and that of  $i$  are correlated, the linear correlation coefficient between  $\gamma_T$  and  $\gamma_i$  being  $r_\gamma = 0.67$  ( $p\text{-value} = 0.001$ ). This indicates an inter-dependence between the variations in skewness of the time-interval distribution and that of the leading digit distribution, that occur at different dynamical transitions.

To quantify how closely the system obeys BL in the different dynamical regimes, we show the results of different statistical tests for goodness of fit between the em-

pirical and Benford distributions. Fig 5 (A) shows the Kolmogorov-Smirnov (KS) test statistic as a function of the  $\text{Ca}^{2+}$  channel conductance  $G_{si}$  which clearly indicates that the distribution of leading digits follow BL most closely, indicated by dips in the test statistic, at the values of  $G_{si}$  characterizing the different dynamical transitions, viz.,  $G_{si} = 0.025, 0.04$  and  $0.055$ . Note that low values of the KS test statistic (i.e., better agreement with BL) are associated with high positive skewness of the distribution of leading digits of the normalized intervals. This is underlined by the strong negative correlation between the test statistic  $k$  and the skewness  $\gamma_i$  (see Fig. 5 B), having a linear correlation coefficient  $r = -0.96$  ( $p = 10^{-12}$ ). As mentioned earlier, this is consistent with

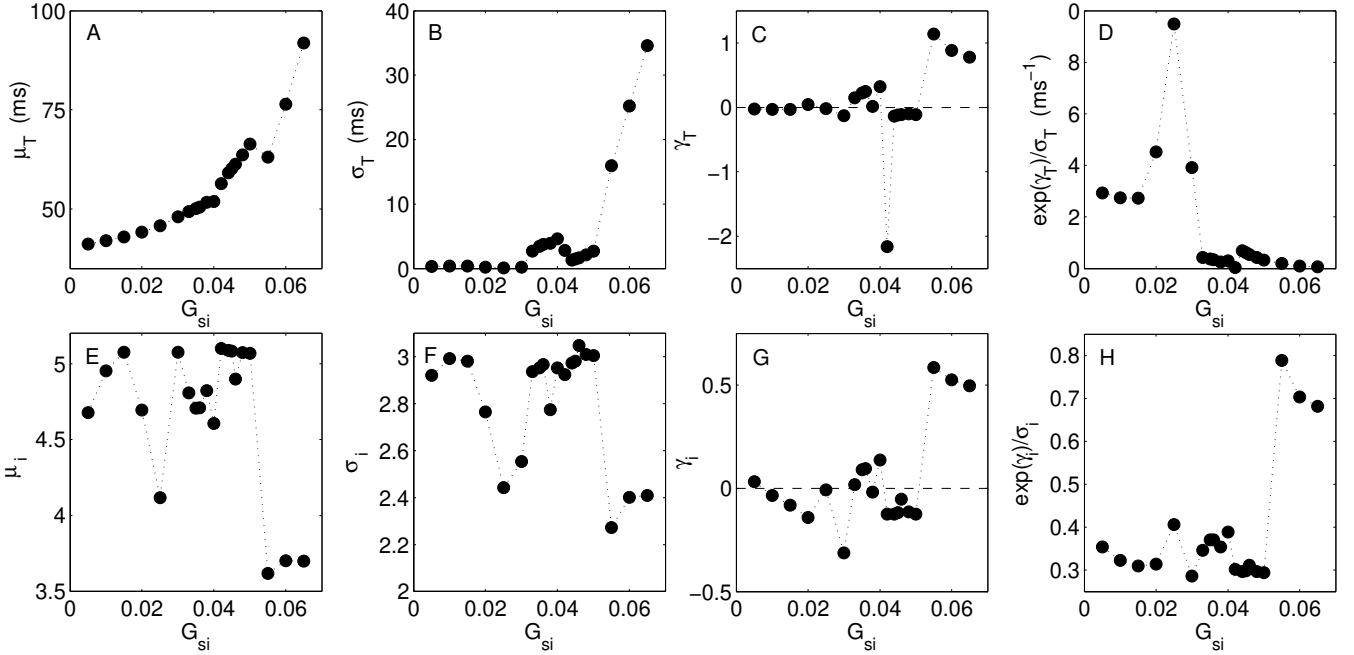


FIG. 4: Analysis of various moments for the distributions of the time intervals  $T$  between successive supra-threshold activations of a local region (A-D) and that of the leading digits  $i$  of the normalized time intervals (E-H) as a function of the maximum  $\text{Ca}^{2+}$  channel conductance  $G_{si}$ . Variation in (A) the mean  $\mu_T$ , (B) standard deviation  $\sigma_T$ , (C) skewness  $\gamma_T$  measured in terms of the Pearson's moment coefficient and (D) the derived quantity  $\exp(\gamma_T)/\sigma_T$ , correspond to the distribution of the time intervals  $T$ , while the variation shown for (E) the mean  $\mu_i$  (F) standard deviation  $\sigma_i$ , (G) skewness  $\gamma_i$  (again measured in terms of the Pearson's moment coefficient) and (H) the quantity  $\exp(\gamma_i)/\sigma_i$ , correspond to the distribution of the leading digits  $i$ . Large changes in both the skewness measures ( $\gamma_T$  and  $\gamma_i$ ), and to an extent, the dispersion measures ( $\sigma_T$  and  $\sigma_i$ ) correspond to successive dynamical transitions between rigid rotation, quasiperiodic meander and chaotic meander of the spiral core, finally giving rise to spatiotemporal chaos resulting from spiral breakup. The measure  $\exp(\gamma_i)/\sigma_i$  combines the information obtained from the variation of standard deviation and skewness, enabling it to indicate some of the the dynamical transitions more clearly. All values shown are obtained by averaging over  $> 2 \times 10^3$  values (chosen far from the spiral core to avoid measurement artifacts). The linear correlation coefficient between the skewness of  $T$  and that of  $i$  is  $r_\gamma = 0.67$  (p-value= 0.001).

the fact that BL is associated with distributions having high positive skewness. Fig. 5 (C) shows the result of another statistical test, viz., Pearson's Chi-squared test, with the lowest values of Pearson's error - corresponding to better agreement with BL - occurring at the same values of  $G_{si}$  where the dynamical transitions occur. The points at which the empirical distribution best matches BL are seen to be consistent for the two tests (the dips of the two test statistics occurring at the same values).

To summarize the results, around the parameter values where the transitions between dynamical regimes representative of different types of cardiac arrhythmia occur, we observe both higher positive skewness and closer agreement with BL (as indicated by statistical tests). We note that both increased skewness and better match with BL have independently been suggested earlier as possible signatures for dynamical transitions, although not in the context of physiology or clinical applications. Apart from the potential utility of this observation for devising robust indicators of the onset of life-threatening disturbances in the cardiac rhythm, it suggests a deep relation between the appearance of BL in natural phenomena and

the degree of skewness in the distributions of the underlying variables.

#### IV. DISCUSSION

Statistical analysis of data (in particular, ECG) that is representative of cardiac functionality can provide us with effective signatures for the detection of arrhythmia at an early stage. Despite such analyses, certain kinds of arrhythmia fail to get detected merely due to the complexity involved. Part of the difficulty lies in cardiovascular activity being a joint outcome of intrinsic spatiotemporal excitation dynamics in heart muscle and modulation of the sinus node by the sympathetic and parasympathetic nervous system. Here we have studied a biophysically detailed model of ventricular activity to infer signatures of dynamical transitions characterizing the onset of different kinds of arrhythmia. This makes it possible to disentangle the effects of intrinsic excitation dynamics in the heart from the influence of the nervous system. In principle, it allows identification of patterns

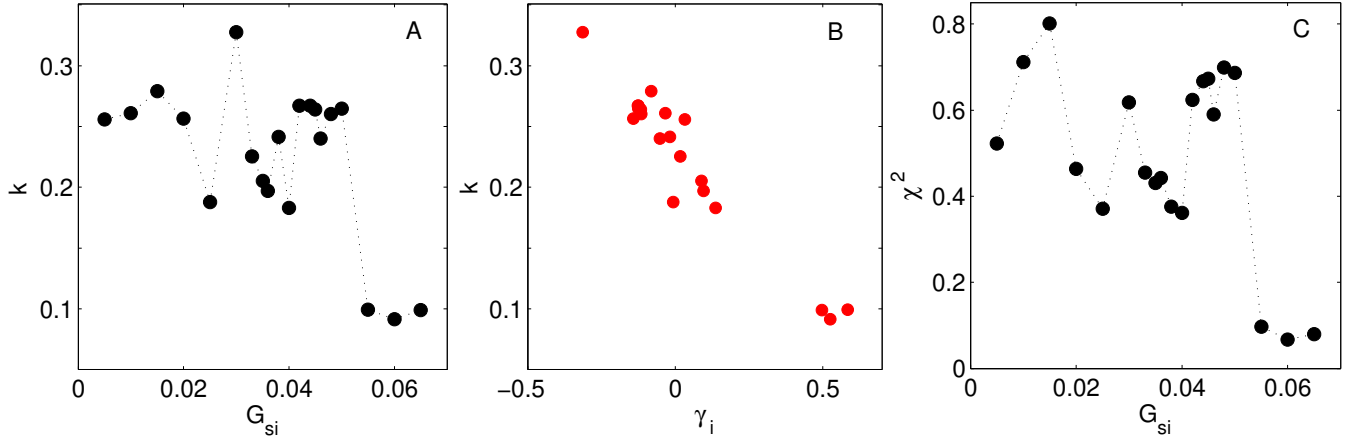


FIG. 5: (A) Deviation of the distribution of leading digits  $i$  of the normalized time intervals  $t$  from Benford's law measured in terms of the Kolmogorov-Smirnov test statistic  $k$  and shown as a function of the maximum  $\text{Ca}^{2+}$  channel conductance  $G_{si}$ . (B) shows that there is a strong negative correlation ( $r = -0.96$ ,  $p$ -value =  $10^{-12}$ ) between  $k$  and the skewness of the leading digits  $\gamma_i$ . (C) The error in using BL for describing the empirical distribution of leading digits  $i$  of the normalized time intervals  $t$  is measured using Pearson's chi-square test and shown as a function of  $G_{si}$ . Agreement with BL improves whenever there is a dynamical transition, as seen by dips in  $k$  and the  $\chi^2$  test statistic for values of  $G_{si}$  where successive transitions between rigid rotation, quasiperiodic meandering and chaotic meandering of the spiral core and spatiotemporal chaos occur. Data points shown are averaged over  $> 2 \times 10^3$  values (chosen far from the spiral core to avoid measurement artifacts).

that may alert one to impending harmful disruptions in the rhythmic activity of the heart, but which could be masked in the ECG signal by autonomic modulation effects. Our results show that as the spatiotemporal excitations in the ventricles become more disordered, leading to phenomena identified with tachycardia and fibrillation, these transitions are marked by characteristic changes in statistical moments associated with the distribution of inter-activation intervals. In addition, the leading digits of these intervals show a closer agreement with BL at the transition points. Our result can potentially be applied in augmenting algorithms used in implanted devices (ICDs) for detecting transitions to possible life-threatening arrhythmia so as to initiate a program of treatment [46]. Thus, when continual monitoring of heartbeat time-series shows either increased skewness or a closer agreement to BL, it may signal a transition in the dynamical state of the heart so that suitable pacing therapy can be started.

Examining the passage from normal cardiac activity to different arrhythmic regimes from the perspective of phase transitions can provide novel insights, as has been pointed out by several earlier studies. For instance, power-law behavior, which characterize critical phenomena in physical systems, have been reported in R-R interval fluctuations and are seen to be remarkable predictors of arrhythmic death, with a steeper negative slope of the power spectra (in log scale) clearly distinguishing a diseased heart from a healthy one [47]. More recently, it has been shown that phase transition-like dynamics is exhibited by healthy human heart rate, indicated by long range correlations which is a hallmark of criticality [48]. In contrast, the dynamics of an abnormal heart rate reveals

significant digression from critical behavior. In addition, scale invariance, which is seen in systems close to critical point, has been shown to be indicative of a healthy heart - with its absence being a statistical feature that can alert us about pathological conditions [49]. Our results provide yet another connection between onset of arrhythmia and phase transitions by showing that sharp changes in the skewness of the distribution of dynamical variables, that has previously been associated with dynamical transitions in other systems [33, 34], can potentially act as a robust indicator of transitions between monomorphic tachycardia, polymorphic tachycardia and fibrillation in the heart.

As mentioned earlier, the appearance of BL has also been linked to phase transitions in physical systems [35]. As the Benford distribution follows from requirement of scale invariance of the underlying numbers [41], it is tempting to connect this with the scale invariance of distribution of dynamical variables associated with critical points at which transitions occur. We observe from our results that parameter regimes that give rise to relatively broad distributions of the time-intervals (as is the situation for spatiotemporally chaotic states) show better agreement with BL than those associated with highly confined distributions (as in the case of a rigidly rotating spiral). However, the occurrence of chaos in dynamical systems by itself does not guarantee that BL will be obeyed [42]. Thus, it appears that the appearance of Benford distribution is more closely associated with the onset of dynamical transitions rather than the specific nature of the dynamical states on either side of the transition point. We also note that distributions that follow

BL are, in general, associated with high skewness [50]. This suggests that the highly skewed nature of distributions during dynamical transitions and the observation of better agreement with BL at those points may not be independent of each other. Thus, our results imply that the increased skewness associated with regime shifts and the appearance of Benford distribution during phase transitions - which have been reported earlier in different contexts - are, in fact, related.

Our work also helps in understanding why, on the one hand, transition to different types of arrhythmia from normal function in the heart is associated with increasingly irregular dynamics of cardiac activity, and yet, on the other hand, healthy subjects appear to show more complex ECG patterns than those suffering from various cardiac diseases. We have shown this by analyzing the behavior of our model system in different arrhythmic regimes through multifractal methods used for quantifying the dynamical complexity of the excitation patterns recorded in ECGs. Our results show that, taken in isolation, the intrinsic behavior of the cardiac muscle becomes more complex as the spatiotemporal dynamics becomes more irregular, with rigidly rotating spirals (representing monomorphic tachycardia) giving way to meandering vortices (suggestive of polymorphic tachycardia) and spatiotemporal chaos (indicating the onset of fibrillation). This contrasts with observations made from multifractal analysis of heart rate recordings in human subjects that, characterization of healthy hearts require

multiple exponents while a single exponent - indicative of monofractality - is sufficient to describe diseased heart behavior [51]. A related measure of dynamical complexity, viz., entropy, has also been shown to be higher in subjects with a heart disease relative to healthy subjects, and suggested as a signature of cardiac abnormality [52]. Comparison of these reports based on analysis of data recorded from live subjects with our simulation results (that did not involve any autonomic modulation of cardiac activity) suggests a possibly critical role played by the interaction of the heart with the nervous system in making the dynamics of the healthy heart appear more complex than abnormal cardiac behavior.

### Acknowledgments

We are grateful to Ujjwal Sen who has been instrumental in getting us interested in the possibility of observing BL in cardiac phenomena. We would also like to thank Indrani Bose, K. Chandrashekhar and Shakti N. Menon for several helpful suggestions. This research was supported in part by the IMSc Complex Systems (XII Plan) Project funded by the Department of Atomic Energy, Government of India. We thank the HPC facility at IMSc for providing access to “Satpura” which is partly funded by DST (Grant No. SR/NM/NS-44/2009).

---

[1] L. Glass, *Nature (London)* **410**, 277 (2001).

[2] D. P. Zipes and J. Jalife, *Cardiac Electrophysiology: From Cell to Bedside*, 6th edition (Elsevier Saunders, Philadelphia, 2013).

[3] A. T. Winfree, *The Geometry of Biological Time*, Springer-Verlag, New York, NY, 1980.

[4] M. C. Mackey and L. Glass, *Science* **197**, 287 (1977); *Dynamical disease: Mathematical analysis of human illness*, edited by J. Bélair, L. Glass, U. an der Heiden and J. Milton (American Institute of Physics, New York, 1995).

[5] M. Heron, *National Vital Statistics Reports* **62**, 1 (2013)

[6] C. H. Hennekens, *Circulation* **97**, 1095 (1998).

[7] Z.-J. Zheng, J. B. Croft, W. H. Giles and G. A. Mensah, *Circulation* **104**, 2158 (2001).

[8] S. R. Madhavan, S. Reddy, P. K. Panuganti, R. Joshi, J. Mallidi, K. Raju, K. R. Raju, S. Iyengar, K. S. Reddy, A. Patel, B. Neal, N. Calambur and H. Tandri, *Indian Pacing Electrophysiol. J.* **11**, 93 (2011).

[9] B. H. Rao, B. K. Sastry, S. S. Chugh, S. Kalavakolanu, J. Christopher, D. Shangula, R. Korabathina and P. K. Raju, *Int. J. Cardiol.* **154**, 163 (2012).

[10] L. S. Gold, C. E. Fahrenbruch, T. D. Rea and M. S. Eisenberg, *Resuscitation* **81**, 622 (2010).

[11] A. H. Travers, T. D. Rea, B. J. Bobrow, D. P. Edelson, R. A. Berg, M. R. Sayre, M. D. Berg, L. Chameides, R. E. O’Connor and R. A. Swor, *Circulation* **122**, S676 (2010).

[12] D. J. Christini, F. M. Bennett, K. R. Lutchen, H. M. Ahmed, J. M. Hausdorff and N. Oriol, *IEEE Trans. Biomed. Eng.* **42**, 411 (1995).

[13] J. Kurths, A. Voss, P. Saparin, A. Witt, H. J. Kleiner and N. Wessel, *Chaos* **5**, 88 (1995).

[14] A. L. Goldberger, C.-K. Peng and L. A. Lipsitz, *Neurobiol. Aging* **23**, 23 (2002)

[15] A. Voss, S. Schulz, R. Schroeder, M. Baumert and P. Caminal, (2009). *Phil. Trans. Roy. Soc. A* **367**, 277 (2009).

[16] M. M. Wolf, G. A. Varigos, D. Hunt and J. G. Sloman, *Med. J. Aust.* **2**, 52 (1978).

[17] R. E. Kleiger, J. P. Miller, J. T. Bigger and A. R. Moss, *Am. J. Cardiol.* **59**, 256 (1987).

[18] F. Lombardi, *Circulation* **101**, 8 (2000).

[19] M. Costa, A. L. Goldberger and C. K. Peng, *Phys. Rev. Lett.* **89**, 068102 (2002).

[20] A. Garfinkel, P. S. Chen, D. O. Walter, H. S. Karagueuzian, B. Kogan, S. J. Evans, M. Karpoukhin, C. Hwang, T. Uchida, M. Gotoh, O. Nwasokwa, P. Sager and J. N. Weiss, *J. Clin. Invest.* **99**, 305 (1997).

[21] M. Small, D. Yu, J. Simonotto, R. G. Harrison, N. Grubb and K. A. A. Fox, *Chaos Solitons Fractals* **13**, 1755 (2002).

[22] T. Nakai, Y. Hirata, S. Horai, M. Akagi and K. Aihara, *Int. J. Bif. Chaos* **20**, 4151 (2010).

[23] J. N. Weiss, A. Garfinkel, H. S. Karagueuzian, Z. Qu and P.-S. Chen, *Circulation* **99**, 2819 (1999).

[24] F. H. Fenton, E. M. Cherry, H. M. Hastings and S. J. Evans, *Chaos* **12**, 852 (2002).

[25] S. Sridhar, A. Ghosh and S. Sinha, *EPL* **103**, 50003 (2013).

[26] S. Sinha and S. Sridhar, *Patterns in Excitable Media*, CRC Press, Boca Raton, FL, 2015.

[27] F. Lombardi and P. K. Stein, *Frontiers in Physiology* **2**, 95 (2011).

[28] D. Purves, G. J. Augustine, D. Fitzpatrick, L. C. Katz, A-S. LaMantia, J. O. McNamara and S. M. Williams (eds.), *Neuroscience*, Sinauer, Sunderland, MA, 2001.

[29] T. P. Hill, *Am. Sci.* **86**, 358 (1998).

[30] M. Sambridge, H. Tkalčić and A. Jackson, *Geophys. Res. Lett.* **37**, L22301 (2010).

[31] J. L. Friar, T. Goldman and J. Pérez-Mercader, *PLoS One* **7** e36624 (2012).

[32] M. J. Nigrini, *J. Am. Tax Assoc.* **18**, 72 (1996).

[33] V. Guttal and C. Jayaprakash, *Ecol. Lett.* **11**, 450 (2008).

[34] M. Scheffer, J. Bascompte, W. A. Brock, V. Brovkin, S. R. Carpenter, V. Dakos, H. Held, E. H. van Nes, M. Rietkerk and G. Sugihara, *Nature (Lond.)* **461**, 53 (2009).

[35] A. S. De and U. Sen, *EPL* **95**, 50008 (2011).

[36] C. H. Luo and Y. Rudy, *Circ. Res.* **68**, 1501 (1991).

[37] F. Xie, Z. Qu, A. Garfinkel and J. N. Weiss, *Am. J. Physiol. Heart Circ. Physiol.* **280**, H535 (2001).

[38] D. Barkley, M. Knob, and L. S. Tuckerman, *Phys. Rev. A* **42**, 2489 (1990).

[39] J. W. Kantelhardt, S. A. Zschiegner, E. Koscielny-Bunde, S. Havlin, A. Bunde, H. E. Stanley, *Physica A* **316**, 87 (2002).

[40] R. M. Fewster, *Am. Stat.* **63**, 26 (2009).

[41] T. P. Hill, *Statist. Sci.* **10**, 354 (1995).

[42] C. R. Tolle, J. L. Budzien and R. A. LaViolette, *Chaos* **10**, 331 (2000).

[43] M. A. Snyder, J. H. Curry and A. M. Dougherty, *Phys. Rev. E* **64**, 026222 (2001)

[44] Z. Qu, F. Xie, A. Garfinkel and J. N. Weiss, *Annals Biomed. Engg.* **28**, 755 (2000).

[45] Y. Ashkenazy, *Physica A* **323**, 19 (2003).

[46] S. A. C. Schuckers, *J. Electrocardiology* **31**, 101 (1998).

[47] J. T. Bigger, R. C. Steinman, L. M. Rolnitzky, J. L. Fleiss, P. Albrecht and R. J. Cohen, *Circulation* **93**, 2142 (1996).

[48] K. Kiyono, Z. R. Struzik, N. Aoyagi, F. Togo and Y. Yamamoto, *Phys. Rev. Lett.* **95**, 058101 (2005).

[49] K. Kiyono, Z. R. Struzik, N. Aoyagi, S. Sakata, J. Hayano and Y. Yamamoto, *Phys. Rev. Lett.* **93**, 17 (2004).

[50] P. D. Scott and M. Fasli, *Univ. Essex CSM Tech. Rep.* **349** (2001).

[51] P. C. Ivanov, L. A. N. Amaral, A. L. Goldberger, S. Havlin, M. G. Rosenblums, Z. R. Struzik and H. E. Stanley, *Nature* **399**, 461 (1999).

[52] T. H. Makikallio, T. Seppanen, M. Niemela, K. E. Airaksinen, M. Tulppo and H. V. Huikuri, *J Am Coll Cardiol* **4** 1005 (1996).